

Natural resonance frequencies, wave blocking, and energy localization in an elastic half-space and waveguide with a crack

Evgeny Glushkov^{1,a}, Natalia Glushkova¹, Michael Golub¹, and Anders Boström²

¹*Department of Applied Mathematics, Kuban State University, Krasnodar, 350040 Russia*

²*Department of Applied Mechanics, Chalmers University of Technology, SE-412 96 Göteborg, Sweden*

(Received 5 October 2005; revised 10 March 2006)

Running title: Glushkov *et al.*: Energy localization in elastic waveguides

^aElectronic mail: evg@math.kubsu.ru

Sharp stopping of time-harmonic wave transmission in elastic structures with defects is considered as a manifestation of the well-known trapped mode effect. It is associated with natural resonance poles lying close to the real axis in the complex frequency plane. Non-resonant wave blocking may also occur due to antiphase combination of the incident and scattered waves. The present paper is aimed to give an insight into such phenomena using an analytically based computer model which strictly takes into account all wave interactions in a cracked structure. Numerical examples are restricted to the case of a line horizontal crack in a half-plane or in a layer (2D in-plane motion), that is, nevertheless, quite enough to demonstrate two kinds of the Rayleigh wave stopping mechanisms (resonant and non-resonant) as well as a possibility of pure real natural resonance frequencies and of a full blocking effect with energy localization.

PACS numbers: 43.20.Gp, 43.20.Ks, 43.20 Mv

I. INTRODUCTION

The diffraction of traveling waves by a subsurface defect sometimes entails a sharp growth of the surface displacement above the obstacle. Conventionally such a phenomenon is explained by the trapped mode effect^{1, 2}, featured by the wave energy localization near the obstacle. Mathematically, the trapped mode occurs when a spectral point ω_n of the boundary value problem modeling a time-harmonic wave process $\mathbf{u}e^{-i\omega t}$ lies close to the real axis $\text{Im}\omega = 0$ in the complex frequency plane. Excitation of the structure at frequencies $\omega \approx \text{Re}\omega_n$ with $|\text{Im}\omega_n|/\text{Re}\omega_n \ll 1$ gives rise to resonance effects such as wave trapping and screening. The rigorous mathematical foundation of resonance classification for inhomogeneous elastic waveguides is grounded by I.I.Vorovich^{3, 4}. Besides the resonance effects an antiphase combination of incident and diffracted waves can also result in non-resonant stopping of the wave transmission.

With regard to practical applications, there exists a strong interest in studying the elastodynamic scattering by crack-like obstacles. It is of importance both to the development of crack detection methods and to the assessment of a possible failure due to resonance effects.

Investigations of the location of the resonance poles in the complex ω -plane for a crack in an unbounded elastic space^{5, 6, 7} has shown that ω_n lies rather far from the real axis. Obviously, in the presence of boundaries, providing additional wave fields reflected recurrently from the crack and boundary surfaces, the location of ω_n changes so that in some situation $|\text{Im}\omega_n|$ may become very small. Therefore, the first goal of our work is to trace the poles in the complex plane as the crack changes its size or approaches the surface. The prime question here is: is it even possible to have a purely real spectral point ω_n ? Accompanying questions are: what happen at resonant frequencies regarding to wave transmission by and energy localization near the crack; what is the mechanism

of wave blocking; is it even possible to have a full stopping of traveling wave transmission by a sub-surface obstacle?

Traditionally the mathematical modeling in non-destructive evaluation relies on the ray methods of the geometrical theory of diffraction (GTD) which operates with physically evident wave expressions. Unfortunately, these methods are not suitable to clear up these questions due to the limits of their asymptotic nature. On the other hand, the direct numerical methods based on the mesh discretization of a solid volume are too time-consuming and cannot provide an insight into the wave structure of the solution.

To address the questions stated above we rely on the analytically based computer model developed earlier for the purposes of ultrasonic crack detection ⁸. Within this model the incident and scattered fields are expressed in terms of path Fourier integrals and their asymptotics via Green's matrices of the structures considered, given source characteristics (loads) and unknown crack opening displacements (c.o.d.). The latter are found from the boundary integral equations (BIEs) implied by the boundary conditions at the crack sides.

The use of the integral equation approach for the problem considered is justified, therefore, by the fact that it holds an intermediate position between the ray and direct numerical methods. First, it provides the same quantitative solution like FEM or Finite Differences, but with much lower costs. Then, it is easily applicable to infinite domains (open waveguides) and asymptotics derived from the integral representations give the same physically significant expressions as ray-based approaches, while keeping in contrast all the comprehensive information about sources, structures and scatters. These asymptotics are quite appropriate for the GTD as well.

Though the developed model ⁸ provides rigorous 3D elastodynamic solutions for arbitrarily shaped and inclined cracks in layered structures, in the present work we limit

ourselves to 2D in-plane diffraction problems for horizontal strip-like (line) cracks. It is quite sufficient for examining the wave effects of interest.

Earlier we already considered blocking effects associated with the diffraction by obstacles of a different nature. The investigation into the fine structure of energy fluxes in an elastic layer with a surface rigid obstacle helped us, for example, in understanding the role of energy vortices in these processes ^{9, 10}. The first results for the blocking by a crack in a half-space are given in the recent short communication ¹¹, then the investigation for a crack in a layer is started ¹². The present work summarizes and develops those previous results. The main distinctive attainment is the discovery of pure real spectral points ω_n and the analysis of the eigensolutions yielding wave localization.

The description of the mathematical technique used is available in the papers mentioned above. Therefore, in the next section II we give only a brief description of the model sufficient for understanding the results. Nevertheless, the explicit analytical representations of Green's matrices for the structures considered, that may be of independent interest, are attached in the Appendix.

Then, in section III, we focus on the Rayleigh wave diffraction by a horizontal crack in a half-plane. With this simplest model we consider typical situations of wave transmission stopping and energy localization. The most remarkable fact discovered here is a possibility of a full Rayleigh wave blocking without any energy trapping (non-resonant antiphase annihilation); whereas the resonance poles ω_n yield strong energy localization. They are not purely real and do not assure, therefore, the complete wave blocking in a half-plane.

For a layer the dependence of the transmission coefficient on geometry (crack's width and depth) and frequency is much more complicated. The examples of section IV show a crucial role of the resonance poles for the transmission control in layer waveguides. In contrast to the half-plane structure, examples of purely real poles ω_n as well as examples

of a full resonant blocking have been found here. As is to be expected, the calculation of displacement eigenforms associated with the real spectral points ω_n shows strong wave localization near the crack. Hence, a sharp resonant blocking at $\omega \approx \text{Re}\omega_n$ is easily explicable by the fact that in such a case the most part of wave energy is distributed to the dominating eigenform featured by a sharp localization around the crack.

II. MATHEMATICAL MODEL

Let us consider an in-plane steady-state harmonic oscillation $\mathbf{u}(\mathbf{x})e^{-i\omega t}$ ($\mathbf{u} = (u_x, u_z)$) of an elastic isotropic layer of thickness H , governed by the Lamé equations

$$(\lambda + \mu)\nabla\text{div}\mathbf{u} + \mu\Delta\mathbf{u} + \rho\omega^2\mathbf{u} = 0.$$

Here and below, due to linearity of the governing relations, the harmonic multiplier $e^{-i\omega t}$ is conventionally omitted. The material properties are specified by Lamé constants λ , μ and density ρ .

The layer contains a subsurface horizontal line crack of width $2a$ at the depth d from the upper surface (Fig 1a). The thickness H may be infinite ($H = \infty$), in such a case we deal with a half-plane (Fig. 1b).

In the Cartesian coordinate system $\mathbf{x} = (x, z)$ the layer occupies the domain $|x| \leq \infty, -H \leq z \leq 0$. The crack is modeled by an infinitesimally thin cut along a line segment $|x| \leq a, z = -d$ with stress-free sides:

$$\boldsymbol{\tau}|_{z=-d} = 0, \quad |x| < a, \tag{1}$$

here $\boldsymbol{\tau} = (\tau_{xz}, \sigma_{zz})$ is the stress vector at a horizontal surface element. The displacement vector is discontinuous on the crack with an unknown jump (c.o.d.)

$$\mathbf{v}(\mathbf{x}) = \mathbf{u}(\mathbf{x})|_{z=-d-0} - \mathbf{u}(\mathbf{x})|_{z=-d+0}. \tag{2}$$

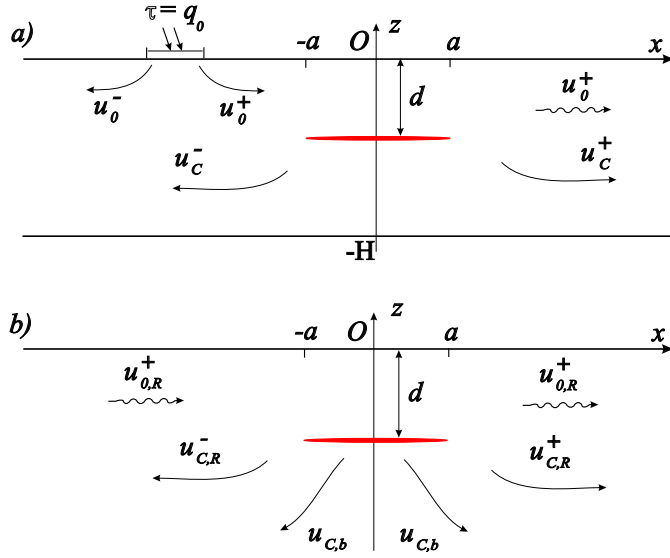


Figure 1: Wave fields' geometry in a layer (a) and a half-plane (b).

It is assumed that the crack sides do not touch each other.

For definiteness let us consider a free waveguide excited by a surface load \mathbf{q}_0 or by an incident wave \mathbf{u}_0^+ coming from infinity. Thus, the sides $z=0$ and $z=-H$ are stress-free except, possibly, at the local source zone $|x-x_0| \leq b$ to which the load \mathbf{q}_0 is applied:

$$\tau|_{z=0} = \begin{cases} \mathbf{q}_0(x), & |x-x_0| \leq b \\ 0, & |x-x_0| > b \end{cases} \quad (3)$$

$$\tau|_{z=-H} = 0, \quad (4)$$

For a half-plane condition (4) is unnecessary.

Finally, for ideally elastic material properties boundary conditions (1) – (4) are to be supplemented by certain radiation conditions assuring the uniqueness. As the radiation condition we use the principle of limiting absorption¹³, which means that the solution for an ideally elastic medium is the limit of the unique solution of the corresponding problem for a medium with attenuation ε as $\varepsilon \rightarrow 0$.

In the presence of a crack the total wave field is made up of the incident field \mathbf{u}_0 and

the field diffracted by the crack \mathbf{u}_c : $\mathbf{u} = \mathbf{u}_0 + \mathbf{u}_c$. Let us mark the part of a wave field propagating in the waveguide from the left to the right by a superscript "plus" (\mathbf{u}_0^+ , \mathbf{u}_c^+), while \mathbf{u}_0^- , \mathbf{u}_c^- are traveling waves going in the opposite direction. For definiteness, let the incident wave come to the crack from the left, i.e. it is \mathbf{u}_0^+ . Consequently, the transmitted field is $\mathbf{u}_0^+ + \mathbf{u}_c^+$ and the reflected one is \mathbf{u}_c^- (Fig. 1). In a half-plane both \mathbf{u}_0 and \mathbf{u}_c contain in addition the body-wave constituents $\mathbf{u}_{0,b}$ and $\mathbf{u}_{c,b}$ radiating downward.

Using the Fourier transform technique with respect to the horizontal coordinate x , \mathbf{u}_0 and \mathbf{u}_c are derived in the form of inverse Fourier integrals

$$\begin{aligned}\mathbf{u}_0 &= \frac{1}{2\pi} \int_{\Gamma} \mathbf{U}_0(\alpha, z) e^{-i\alpha x} d\alpha \equiv \mathcal{F}^{-1}[\mathbf{U}_0] \\ \mathbf{U}_0 &= \int_{-\infty}^{\infty} \mathbf{u}_0(x, z) e^{i\alpha x} dx \equiv \mathcal{F}[\mathbf{u}_0]\end{aligned}\tag{5}$$

Similarly,

$$\mathbf{u}_c = \mathcal{F}^{-1}[\mathbf{U}_c], \quad \mathbf{U}_c = \mathcal{F}[\mathbf{u}_c]$$

By \mathcal{F} and \mathcal{F}^{-1} we denote direct and inverse transforms. The integration path Γ goes in the complex plane α along the real axis $\text{Im } \alpha = 0$ deviating from it for bypassing real poles and branch points of the integrands \mathbf{U}_0 and \mathbf{U}_c in accordance with the principle of limiting absorption ⁴. The solution in the Fourier transform domain is obtained in the form

$$\begin{aligned}\mathbf{U}_0(\alpha, z) &= K(\alpha, z) \mathbf{Q}_0(\alpha) \\ \mathbf{U}_c(\alpha, z) &= M(\alpha, z) \mathbf{V}_0(\alpha)\end{aligned}\tag{6}$$

where $\mathbf{Q}_0 = \mathcal{F}[\mathbf{q}_0]$ and $\mathbf{V} = \mathcal{F}[\mathbf{v}]$ are the Fourier transforms for \mathbf{q}_0 and \mathbf{v} while K and M are transforms of Green's matrices (2×2), whose columns are fields excited by horizontal and vertical surface point loads applied to the surface $z = 0$ (for K) and fields related to horizontal crack-like point sources with shear and normal crack opening displacements (for M). Elements of these matrices are derived in a closed analytical form (see Appendix). In

the analytical calculations we use the technique developed in ⁴; more details of its specific implementation may be also found in the papers ^{8, 10, 11, 14}.

With a layer waveguide $K(\alpha, z)$ and $M(\alpha, z)$ are meromorphic in the complex α -plane matrix-functions. They have a finite number of real poles $\pm\zeta_k, k = 1, 2, \dots, N$ and a countable set of complex ones ($k = N + 1, N + 2, \dots$). The wave fields \mathbf{u}_0^\pm and \mathbf{u}_c^\pm can be expressed as a sum of residues from these poles:

$$\mathbf{u}_0^\pm(\mathbf{x}) = \sum_{k=1}^{\infty} \mathbf{a}_k^\pm(z) e^{\pm i\zeta_k x}, \quad |x - x_0| > b \quad (7)$$

$$\mathbf{u}_c^\pm(\mathbf{x}) = \sum_{k=1}^{\infty} t_k^\pm \mathbf{a}_k^\pm(z) e^{\pm i\zeta_k x}, \quad |x| > a \quad (8)$$

$$\mathbf{a}_k^\pm = \mp i \operatorname{res} K(\alpha, z)|_{\alpha=\mp\zeta_k} \mathbf{Q}_0(\mp\zeta_k), \quad t_k^\pm \mathbf{a}_k^\pm = \mp i \operatorname{res} M(\alpha, z)|_{\alpha=\mp\zeta_k} \mathbf{V}(\mp\zeta_k).$$

The first N terms of these series are related to real poles describing traveling waves (normal modes) propagating along the layer to infinity with the phase and group velocities $c_{p,k} = \omega/\zeta_k$ and $c_{g,k} = d\omega/d\zeta_k$. The rest of the terms decay at infinity as $e^{-|\operatorname{Im} \zeta_k||x|}$, $|x| \rightarrow \infty$. The appearance of dispersion curves $c_{p,k}(\omega)$ and $c_{g,k}(\omega)$ for the layer under consideration is well studied (e.g., see Refs. ^{15, 16}). In the numerical examples considered in section IV below, only the two first fundamental modes a_0 and s_0 exist in the dimensionless frequency range $0 < \omega < \pi$, and three or more traveling waves for $\omega > \pi$.

Whereas the normal modes $\mathbf{a}_k^\pm e^{\pm i\zeta_k x}$ in the expansion (7) are known, the related normal modes for \mathbf{u}_c contain the unknown coefficients t_k^\pm , which are expressed via the unknown c.o.d. \mathbf{v} (more precisely, via $\mathbf{V}(\mp\zeta_k)$ components).

For a half-plane ($H = \infty$) the components of the matrices K and M have two branch points and only one Rayleigh pole ζ , so that in this case

$$\mathbf{u}_0 = \mathbf{u}_{0,R} + \mathbf{u}_{0,b}, \quad \mathbf{u}_c = \mathbf{u}_{c,R} + \mathbf{u}_{c,b}$$

where

$$\mathbf{u}_{0,R}^{\pm} = \mathbf{a}_1^{\pm}(z)e^{\pm i\zeta x}, \quad |x - x_0| > b; \quad \mathbf{u}_{c,R}^{\pm} = t_1^{\pm} \mathbf{a}_1^{\pm}(z)e^{\pm i\zeta x}, \quad |x| > a \quad (9)$$

are Rayleigh waves radiated to infinity from the source and the crack, respectively. The body waves $\mathbf{u}_{0,b}$, $\mathbf{u}_{c,b}$ are represented in terms of integrals over the sides of cuts drawn in the α -plane from the branch points to infinity.

The transmission and reflection coefficients κ^+ and κ^- are introduced as the ratios $\kappa^{\pm} = E^{\pm}/E_0^+$, in which E_0^+ is the absolute value of the time-averaged energy of the waves \mathbf{u}_0^+ incident on the crack, while E^{\pm} are the energy of the transmitted and reflected traveling waves. These energy characteristics are calculated by integrating the horizontal component e_x of the time-averaged power density vector (Umov-Poynting vector) $\mathbf{e} = (e_x, e_z)$ over a vertical cross-section: $E = \left| \int_{-H}^0 e_x(x, z) dz \right|$, $x = \text{const}$. Here $e_x = -(\omega/2) \text{Im}(\mathbf{u} \cdot \boldsymbol{\sigma})$, where $\boldsymbol{\sigma} = (\sigma_{xx}, \tau_{xz})$ is a stress vector at a vertical surface element; as \mathbf{u} we take here \mathbf{u}_0^+ , $\mathbf{u}_0^+ + \mathbf{u}_c^+$ and \mathbf{u}_c^- for E_0^+ , E^+ and E^- respectively. Often only one normal mode of the sum (7) or a single Rayleigh wave (9) is taken as an incident wave \mathbf{u}_0^+ to study its transmission and reflection. In such a case the source is insignificant, we can consider \mathbf{u}_0^+ as a wave coming from minus infinity.

The source characteristics are accounted for in the energy distribution coefficients $\mu^{\pm} = E^{\pm}/E_0$, introduced similarly to κ^{\pm} , but with E_0 to be the source power (total energy radiated into the structure from the load \mathbf{q}_0 : $E_0 = \left| \int_{-\infty}^{\infty} e_z(x, 0) dx \right|$, $e_z = -(\omega/2) \text{Im}(\mathbf{u} \cdot \mathbf{q}_0)$, $\mathbf{u} = \mathbf{u}_0 + \mathbf{u}_c$); E^{\pm} are expressed as above but via $\mathbf{u}_0^{\pm} + \mathbf{u}_c^{\pm}$.

For a half-space the surface-to-body transformation coefficients $\kappa_b = E_b/E_0^+$, $\mu_b = E_b/E_0$ should be introduced in addition (here E_b is the total energy of body waves integrated over the lower semi-circle as its radius $R \rightarrow \infty$). The power conservation law entails the balance equalities $\kappa^+ + \kappa^- + \kappa_b = 1$ and $\mu^+ + \mu^- + \mu_b = 1$. In a layer $E_b, \kappa_b, \mu_b \equiv 0$. The difference between κ^{\pm} and μ^{\pm} becomes apparent taking into consideration that for

a structure without defects $\kappa^+ = 1$ and $\kappa^- = 0$ while $\mu^+ = \mu^-$. With a full blocking $E^+ \equiv 0$, so both κ^+ and μ^+ are equal to zero.

As soon as the Umov-Poynting vector \mathbf{e} is determined at each point \mathbf{x} of the domain, the continuous vector field $\mathbf{e}(\mathbf{x})$ determines in the \mathbf{x} plane non-crossing curves $\mathbf{x} = \mathbf{x}(s)$ to which $\mathbf{e}(\mathbf{x})$ is tangential at any point:

$$\frac{d\mathbf{x}}{ds} = \mathbf{e}(\mathbf{x})/|\mathbf{e}(\mathbf{x})| \quad (10)$$

Here $\mathbf{x} = \mathbf{x}(s)$ is a parametric equation of a curve, s is a natural parameter. Every specific curve passing through a given point x_0 ,

$$\mathbf{x}(0) = x_0 \quad (11)$$

is determined uniquely from the Cauchy problem (10) – (11). These curves, referred to as energy streamlines (similarly to streamlines in fluid dynamics), are used for visualization of time-averaged energy transfer in a harmonic wave field ^{14, 10}, while energy concentration is illustrated by the space distribution of the power density amplitude $|\mathbf{e}(\mathbf{x})|$.

Whereas the incident field \mathbf{u}_0 is known, \mathbf{u}_c is expressed in terms of the unknown c.o.d. $\mathbf{v}(\mathbf{x})$ which is determined by a Wiener-Hopf integral equation

$$\mathcal{L}\mathbf{v} \equiv \int_{-a}^a l(x - \xi)\mathbf{v}(\xi)d\xi = \mathbf{f}(x), \quad |x| < a \quad (12)$$

derived by substituting $\mathbf{u} = \mathbf{u}_0 + \mathbf{u}_c$ in the form (5) - (6) into the homogeneous boundary condition (1) on the crack sides. The hypersingular kernel of this equation $l(x)$ is derived in terms of its Fourier symbol $L(\alpha)$: $l = \mathcal{F}^{-1}[L]$; a specific analytical representation for L is given in Appendix (see eq. A5). The right-hand side $\mathbf{f}(x) = -\boldsymbol{\tau}_0(x, -d)$, where $\boldsymbol{\tau}_0$ is the stress vector at a horizontal area element associated with the incident field \mathbf{u}_0 .

The resonance poles ω_n are spectral points of the integral operator \mathcal{L} . Numerically they are approximated by the roots of the characteristic equation $\det A(\omega) = 0$, where

$A(\omega)$ is the matrix of a linear algebraic system $A\mathbf{t} = \mathbf{f}$ into which Eq. (12) is discretized. There have been developed and implemented a variety of discretization methods such as expansion in terms of splines, orthogonal polynomials or normal modes, reduction to infinite algebraic systems in terms of residuals with their stable truncation (for layered structures), the Wiener-Hopf factorization technique and so on. Each of them is most effective within some specific range of input parameters. Due to their overlapping these approaches provide reasonable results for both small and large frequencies and crack size.

The reliability of the numerical results are controlled by numerically checking the boundary conditions and the power balance, as well as by comparing with known independent results, e.g. with Ref. ¹⁷ for arbitrarily inclined subsurface cracks in a half-plane and with Ref. ¹⁸ for cracks in a layer.

III. THE HALF-PLANE

Let us consider the diffraction of a classical Rayleigh wave $\mathbf{u}_{0,R}$ (9) by a subsurface crack. Within this section we use dimensionless parameters set by the equalities $a = 1$, $v_s = 1$, $\rho = 1$, and Poisson's ratio $\nu = 1/3$. That is, the unit of length is fixed by the crack's semi-width a and the dimensionless angular frequency is $\omega = 2\pi fa/v_s$, where f , a and v_s are dimensional frequency, semi-width and S wave velocity.

First of all, let us consider the location of the poles ω_n in the complex ω -plane. Fig. 2 gives the six natural frequencies closest to the real axis as functions of the depth d (plots $\text{Re}\omega_n(d)$, $\text{Im}\omega_n(d)$ in the left part and the related trajectories $\omega_n(d)$ in the right part of the figure). The plots show that ω_n approach very close to the real axis as $d \rightarrow 0$, but, nevertheless, they do not touch the axis. Therefore, we believe that no real poles ω_n are possible for a half-plane with a crack.

To illustrate their influence on the Rayleigh wave transmission, Fig. 3 presents exam-

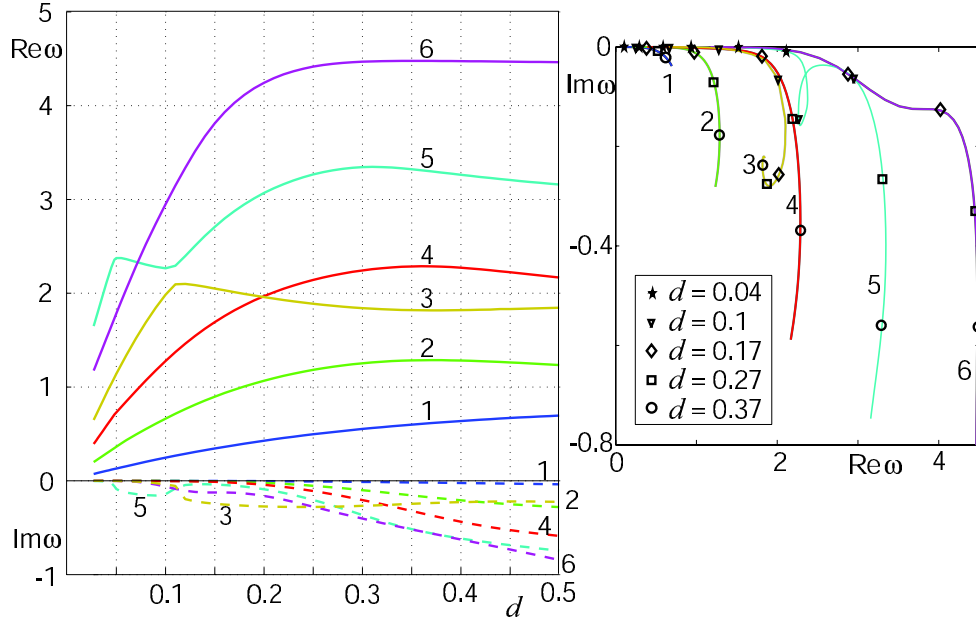


Figure 2: The six complex natural frequencies ω_n closest to the real axis for a half-plane as functions of crack depth d (left) and their trajectories in the ω -plane (right).

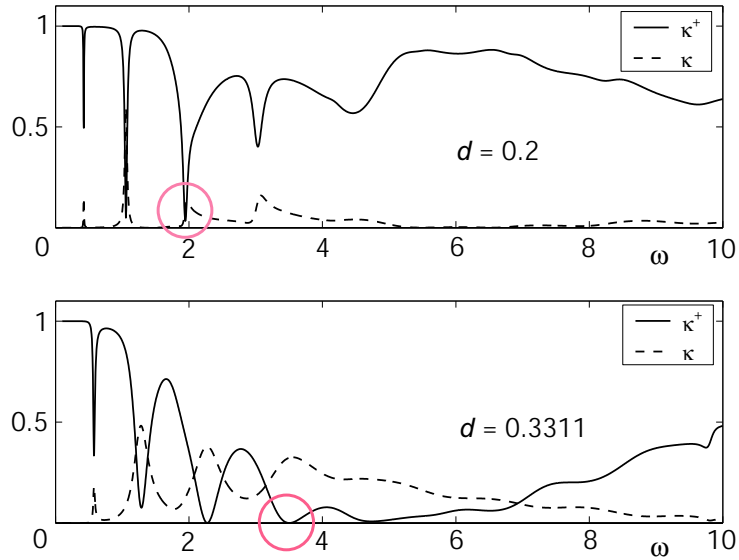


Figure 3: Frequency dependence of the Rayleigh wave transmission and reflection coefficients κ^\pm at different depths d .

ples of typical frequency behavior of the coefficients κ^\pm with two different crack depths d . At $d = 0.2$ one can see narrow dips in the $\kappa^+(\omega)$ plot indicating sharp (resonant) screening of the Rayleigh wave propagation at $\omega = 0.43, 1.07$ and 1.97 . It would appear reasonable that this occurs at $\omega = \text{Re } \omega_n$ for the poles ω_n close to the real axis.

d	ω_1	ω_2	ω_3	ω_4	ω_5	ω_6
0.2	$0.43 - i 0.004$	$1.07 - i 0.02$	$1.96 - i 0.27$	$1.97 - i 0.04$	$3.07 - i 0.09$	$4.24 - i 0.16$
0.3311	$0.58 - i 0.02$	$1.27 - i 0.13$	$1.83 - i 0.25$	$2.26 - i 0.27$	$3.32 - i 0.46$	$4.45 - i 0.47$

Table 1. The six poles ω_n closest to the real axis for the same depths d as in Fig. 3.

Indeed, Table 1, displaying values ω_n for the depths under consideration, shows the same real and very small imaginary parts for $\omega_n, n = 1, 2, 4$ ($d = 0.2$). The poles ω_5 and ω_6 also cause dips in the curve $\kappa^+(\omega)$, which, however, are not so sharp as these points are further away from the real axis.

At $d = 0.331$, wide and deep depressions with minima at $\omega = 3.5$ and 4.8 are added to the dips. There are no complex poles ω_n close to these frequencies, therefore these blocking frequencies are hardly caused by a resonance effect. To illustrate this, we compare surface displacements and energy concentration near the crack at such frequencies with the resonance ones. Examples of the comparison for the two blocking situations marked in Fig. 3 by circles are given in Figs. 4 – 6.

Fig. 4 shows the amplitude of the vertical surface displacement $|u_z|$ at a sharp screening frequency ($\omega = 1.945, d = 0.2$, solid line) and at the minimum of a wide depression ($\omega = 3.505, d = 0.331$, dashed line). In both cases the coefficient κ^+ is very small, therefore, at the right of the crack we see a shadow zone with a minimal surface oscillation decreasing as $x \rightarrow \infty$. Above the crack, in contrast, the surface oscillation exhibits sharp

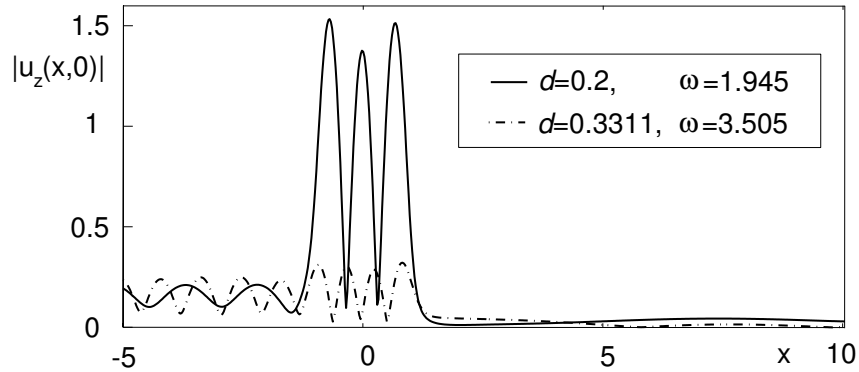


Figure 4: Surface displacement with resonance and antiphase screening.

growth in the first case, while it remains at the same level as in the incoming zone for the second kind of wave blocking. The growth indicates resonance trapping, which is confirmed by the picture of energy localization in Fig. 5.

The energy streamlines in these cases shown in Figs. 5 and 6, respectively, are plotted for the energy flow in the total field $\mathbf{u} = \mathbf{u}_{0,R}^+ + \mathbf{u}_c$, where $\mathbf{u}_{0,R}^+$ is the Rayleigh wave (9) coming from infinity. We should remark that the density of streamlines has no meaning, they only show the trajectories of an averaged energy transfer in a time-harmonic field. The power is specified by the energy density $|\mathbf{e}(\mathbf{x})|$ given in the upper subplots.

In both cases the presence of the crack turns the flow downward, indicating considerable transformation into body waves. As the main difference, there are several energy vortices between the crack and the surface in the first case (see enlarged upper right subplot in Fig. 5). The upper left subplot shows that much more energy density is accumulated in these vortices than in the surrounding field. Hence, it is safe to say that this is a classical trapping with energy localization. The vortices block the way for energy transmission, similarly to the situation in a waveguide with a surface obstacle¹⁰. They leave a space only for a weak energy flow going to infinity along the surface, which results in very small but non-zero κ^+ in this case. It might be worth to remark that so powerful

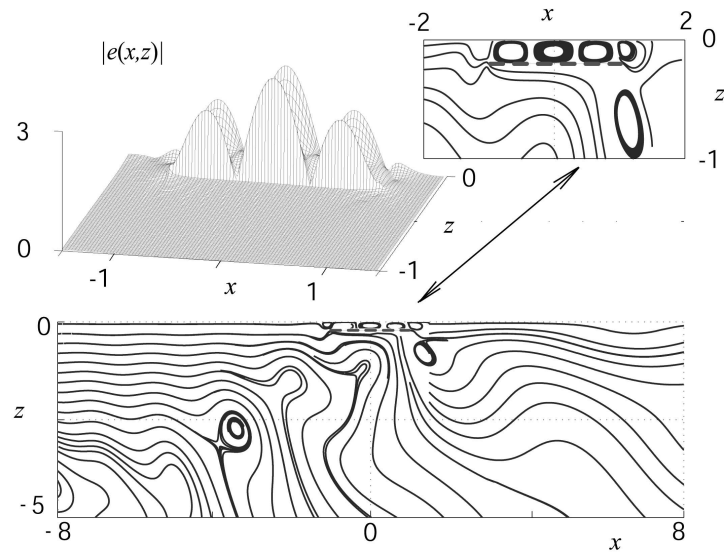


Figure 5: Energy streamlines and power density distribution with a resonant Rayleigh wave trapping ($d = 0.2, \omega = 1.945$).

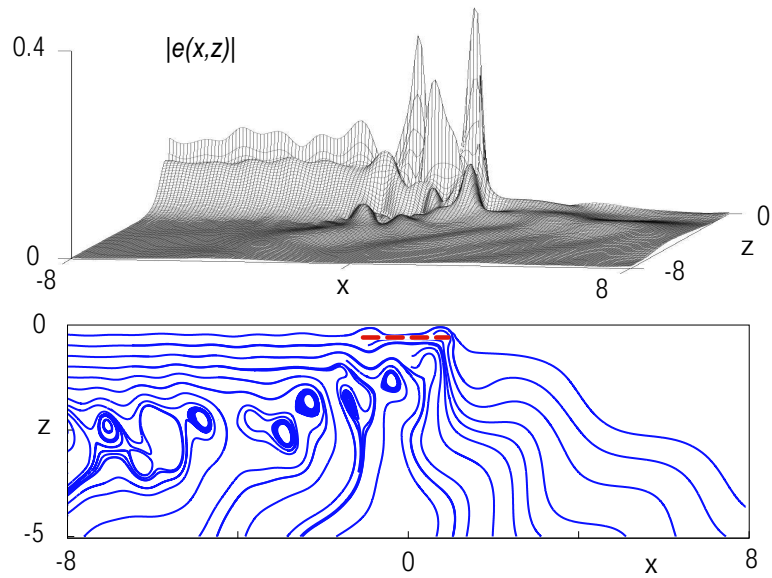


Figure 6: The same with a non-resonant blocking ($d = 0.331, \omega = 3.505$).

vortices, nevertheless, do not upset the total power balance, since they do not contribute to the energy outflow to infinity.

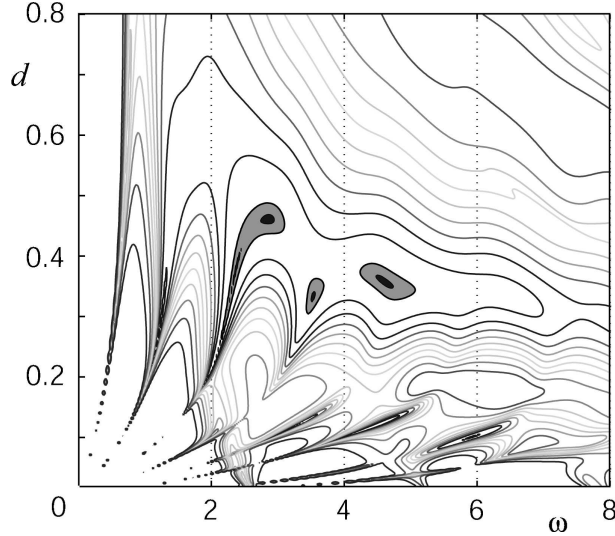


Figure 7: Level lines of the surface $\kappa^+(\omega, d)$ for the incoming Rayleigh wave.

In the second case (Fig. 6) no vortices accumulating energy appear near the crack, but the flow is turned downward so that within numerical accuracy $\kappa^+ = 0$. In the preceding paper ¹¹ we explain this non-resonant stopping by the antiphase annihilation of the incoming and diffracted Rayleigh waves $\mathbf{u}_{0,R}^+$ and $\mathbf{u}_{c,R}^+$ (coefficient t_1^+ in (9) becomes equal to -1 in this case).

Searching for other possible full blocking configurations, we plot the surface κ^+ as a function of ω and d . Fig. 7 shows the level lines of this surface; (its general appearance is also seen in the left subplot of Fig. 9). A characteristic feature of the relief is a deep and wide valley extending from northwest to southeast, approximately from $(\omega, d) = (2, 0.6)$ to $(7, 0.3)$. Grey and black colours indicate zones in which $\kappa^+ \leq 0.01$ and $\kappa^+ \leq 0.001$, respectively.

The global minima of the function κ^+ are sought in these zones, since a deviation

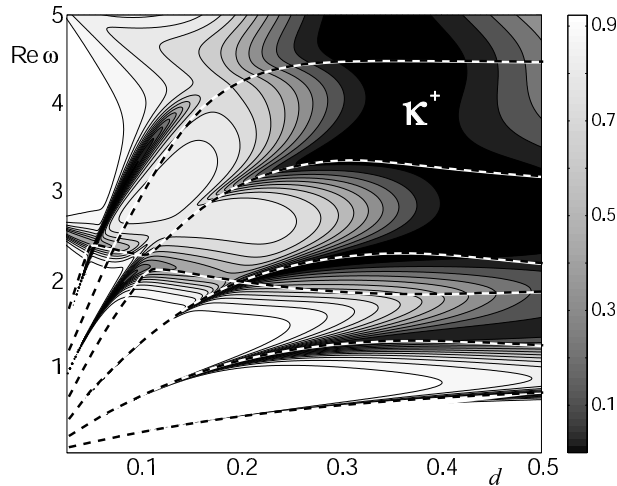


Figure 8: Curves $\text{Re } \omega_n(d)$ as compared with the canyon structure of the surface $\kappa^+(d, \omega)$ (half-plane).

from the valley leads only to an increase in κ^+ . This increase, with κ^+ tending to unity as $\omega \rightarrow \infty$ or $d \rightarrow \infty$, is obviously associated with the fact that with increasing depth-to-wavelength the wave interaction with the crack ceases. A monotonic increase in κ^+ is violated only close to the axis $d = 0$, where the relief becomes very irregular due to almost real ω_n . Therefore, the presence of global minimum points in the band of small d also cannot be totally excluded.

Using a numerical minimization of the function $\kappa^+(\omega, d)$ we find several discrete points in the (ω, d) plane at which the transmission is completely blocked ($\kappa^+ \equiv 0!$). The coordinates of such points for different Poisson's ratios ν are listed in Table 2. The assertion about theoretically complete blocking relies on the numerical results which stably converge to these points with different discretization accuracy. At these points they yield $\kappa^+ \approx 10^{-12} - 10^{-14}$ while in the vicinity $\kappa^+ \approx 10^{-2} - 10^{-4}$.

ν	1	2	3	4
0.1	2.025, 0.433	-	-	-
0.2	2.146, 0.400	3.009, 0.441	3.202, 0.362	-
0.3	2.285, 0.374	2.895, 0.465	3.427, 0.338	-
0.3333	2.337, 0.366	2.849, 0.462	3.509, 0.333	-
0.4	2.450, 0.353	2.739, 0.431	3.689, 0.325	5.036, 0.336

Table 2. The (ω, d) points of the Rayleigh wave complete non-resonant blocking for different Poisson's ratios ν .

As for the blocking due to resonance poles, it appears in narrow canyons, or even slits, in the $\kappa^+(\omega, d)$ relief. This is illustrated in Fig. 8 where the curves $\text{Re } \omega_n(d)$ from Fig. 2 (dashed lines) are put on the surface $\kappa^+(d, \omega)$ (rotated and mirrored part of Fig. 7). We should remark that the canyons are narrower the closer ω_n come to the real axis. That is why they are practically not seen under the curves $\text{Re } \omega_n$ as $d \rightarrow 0$, but they are present, becoming narrower and deeper the smaller $\text{Im } \omega_n$ is. They may be seen as sharp dips on the section profiles $\kappa^+(\omega)$, $d = \text{const}$ (see, e.g., Fig. 3). A certain mismatch of the higher curves with the canyons is apparently due to the presence of the next neighbour poles not shown in this figure.

Thus, there exist two mechanisms of a Rayleigh wave screening by a horizontal subsurface crack. The first one is related to a resonance in the crack-surface system, but it does not ensure complete blocking. The second mechanism results from non-resonant antiphase annihilation of the incident wave and the wave arising due to diffraction. It does not entail any energy trapping and localization, providing, however, complete transmission stopping for certain discrete combinations of the crack depth and frequency.

IV. THE ELASTIC LAYER

Unlike the half-plane, where the surface $\kappa^+(\omega, d)$ provides exhaustive information for the Rayleigh wave transmission, it is hardly possible to give a complete description even for a homogeneous layer. First of all, this is due to a wider range of input parameters (additional thickness H and a richer variety of traveling waves). In addition, the patterns themselves become much more complicated due to multiple recurrent reflections among the crack and the two sides. As an example, the surfaces $\kappa^+(\omega, d)$ for the half-plane considered above ($H = \infty$) and for the layer of thickness $H = 1$ with a crack of semi-width $a = 1$, excited by the first antisymmetric mode a_0 : $\mathbf{u}_0^+ = \mathbf{a}_1^+ e^{i\zeta_1 x}$, are confronted in Fig. 9. Instead of one wide valley we see in the second case a wrinkled surface with a set of slits throughout the entire domain of input parameters.

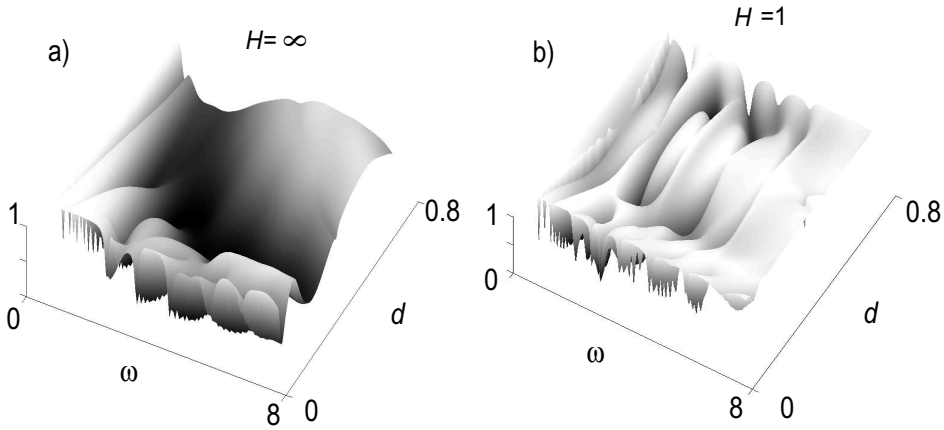


Figure 9: Typical appearance of the surface $\kappa^+(\omega, d)$ for a half-plane (a) and a layer (b).

Considering a layer, it is natural to take its thickness H as a unit of length. Henceforth, within this section $H = 1$, $\omega = 2\pi fH/v_s$ and a may differ from unity; Poisson's ratio $\nu = 1/3$ as above. To avoid a separate consideration for different incoming modes, in some examples we take a multimode incident field \mathbf{u}_0^+ coming from a given vertical point source $\mathbf{q}_0 = (0, \delta(x - x_0))$ (in the examples below $x_0 = -5$). Consequently, the energy distribution coefficients μ^\pm instead of κ^\pm are considered in such a case. Since the poles

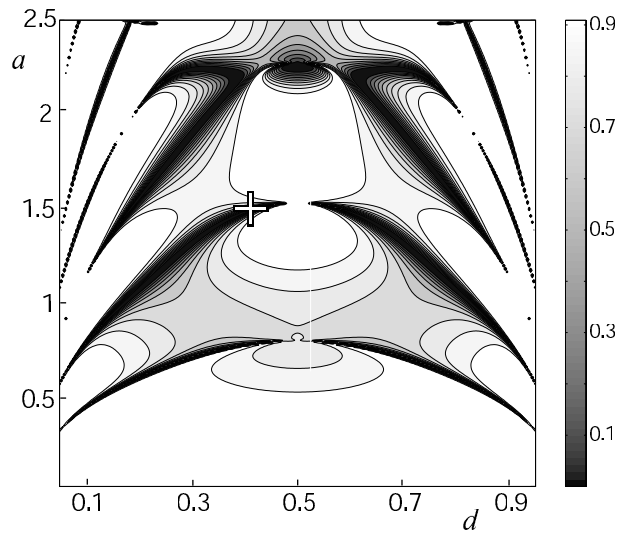


Figure 10: Transmission coefficient κ^+ as a function of a and d at the fixed frequency $\omega = 0.9692$.

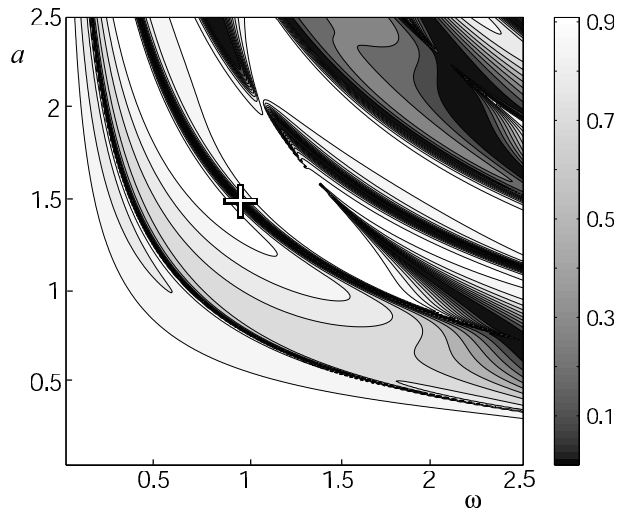


Figure 11: Transmission coefficient κ^+ as a function of ω and a at the fixed depth $d = 0.3994$.

ω_n are independent of \mathbf{u}_0 (as spectral points of the integral operator \mathcal{L} in Eq. (12)) their manifestation in the transmission relationships (canyons) should be the same with any incident field.

Typical examples of the κ^+ dependence on two input parameters with a fixed third one are shown in Figs. 10 – 11 by means of level lines and a grey scale (here the first antisymmetric mode a_0 is taken as \mathbf{u}_0^+). The narrow black strips determine the parameters of resonance blocking. They are analogous to the curves of trapped modes obtained for a fluid layer with a horizontal obstacle¹. As above, a search for the full blocking parameters was organized by numerical minimization of the function κ^+ taking start points at these strips (canyons' bottom).

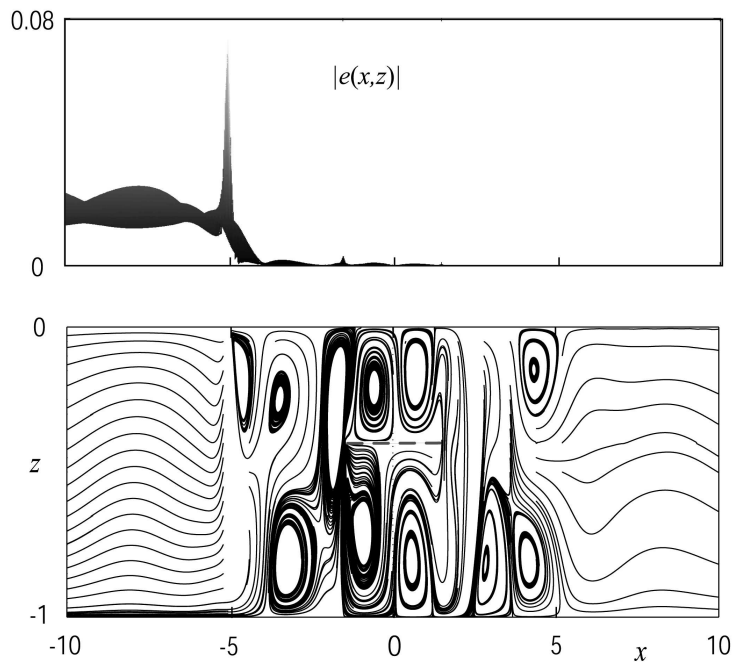


Figure 12: A horizontal profile of the power density surface $|\mathbf{e}(x, z)|$ (a) and energy streamlines (b) from a point source at $x_0 = -5$ for the layer under resonance conditions ($\omega = \text{Re } \omega_n$, $|\text{Im } \omega_n| \ll 1$).

As an example, the minimization from the initial point, marked in Figs. 10 - 11 by a white cross, results in the values $\omega = 0.9692$, $a = 1.4903$ and $d = 0.3994$ for which $\kappa^+ < 10^{-6}$. Nevertheless, we have to note, this is not a case of pure real resonance, because the nearest spectral point ω_n still has a very small imaginary part here. Similar points were found in other parts of the (ω, a, d) space searching over the canyons' bottom. The resonance character of blocking at these points is evident from the sharp local growth of surface displacements above the crack and stress intensity factors at its tips, as well as from energy vortices appearing near the crack. In contrast to the previous example (Fig. 5), with a not distant source these vortices may not accumulate a great power, just turning away to the left the total energy flow incoming from the source (see Fig. 12 for the minimum point (ω, a, d) mentioned above). The horizontal profile of the energy density surface $|\mathbf{e}(x, z)|$ given in the upper subplot shows very small energy amplitudes in the vortex zone. On the other hand, with a distant source or normal modes coming from infinity, a vortex energy concentration at the crack zone, similarly to the half-plane example above, is obtained for a layer as well. It is noted that the vortices, blocking energy transmission by the crack, completely disappear as soon as the point of input parameters displaces slightly across the canyon getting up from its bottom on the brink.

Apparently, the canyons appear due to some near-real ω_n . Similarly to Fig. 8, this is demonstrated by Fig. 13, where plots of $\text{Re } \omega_n(d)$ are put on the level line relief $\kappa^+(d, \omega)$ with $a = 1$, obtained for the incident antisymmetric mode a_0 , which is a Rayleigh wave analog in the layer. For small d the picture becomes similar to the related part of Fig. 8. Obviously, when the crack approaches the upper surface, the influence of the bottom side becomes negligible. For $0.5 \leq d \leq 1$ the picture is mirror symmetric due to the layer symmetry.

In contrast to the half-plane, however, $|\text{Im } \omega_n|$ do not increase monotonously together

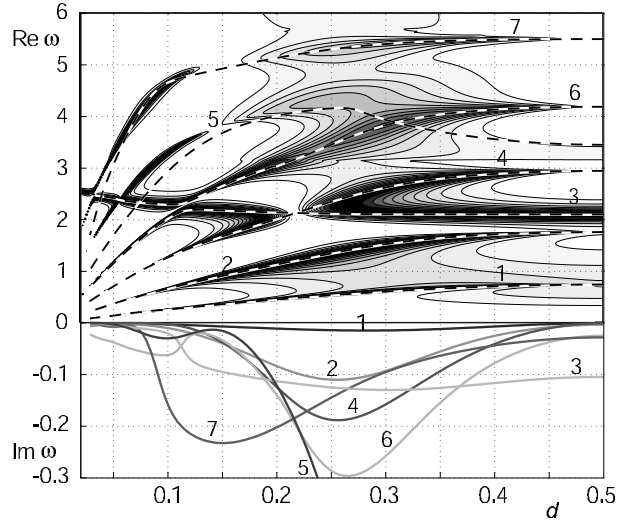


Figure 13: Comparison of pole curves $\text{Re} \omega_n(d)$, $a = 1$ with the canyon structure of the surface $\kappa^+(d, \omega)$ for the layer; the lower part depicts $\text{Im} \omega_n(d)$ in the tenfold enlarged scale.

with d . Some of the poles turn upward and come to the real axis again as $d \rightarrow 0.5$. Similarly to Fig. 8 the canyons are very narrow and practically not seen under the curves $\text{Re} \omega_n$ when ω_n are close to the real axis. But they are present, becoming deeper the smaller $\text{Im} \omega_n$ become, so that in the limit $\kappa^+ = 0$ as $\text{Im} \omega_n = 0$ (i.e. at a pure real resonance frequency).

n	3	5	7	8
ω_n	2.17	1.38	1.95	1.54
a	1.29	1.60	2.84	3.15

Table 3. Real poles ω_n and associated resonance crack widths a for a median crack ($d = 0.5$).

To be certain of the existence of the real poles, we have followed their paths in the complex ω -plane varying a at $d = 0.5$. At certain points of such paths the poles touch

the real axis. Examples of such touching accompanied by complete resonance stopping ($\kappa^+ = \mu^+ \equiv 0$) have been definitely detected (Fig. 14). Values of several pure real poles ω_n found by such a way for different a at the depth $d = 0.5$ are listed in Table 3 together with the resonance crack widths a (the latter are also shown in Fig. 14 by arrows).

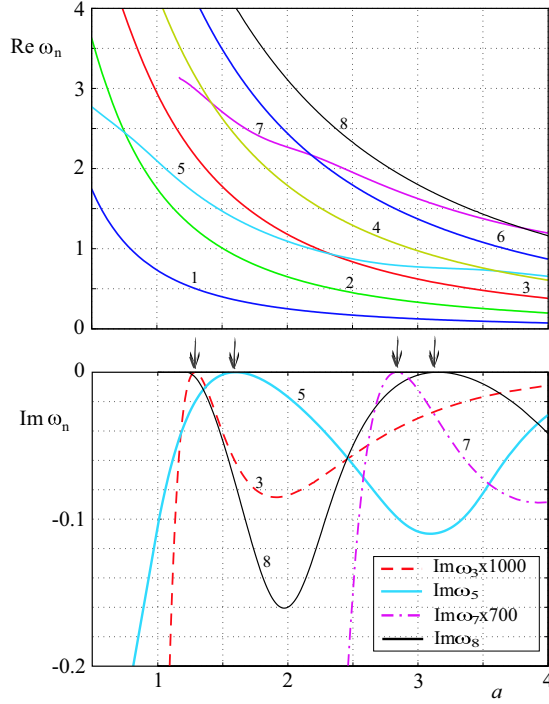


Figure 14: Plots $\text{Re } \omega_n(a)$ (upper) and $\text{Im } \omega_n(a)$ (lower) yielding examples of the natural resonance frequencies ω_n coming up to and touching the real axis $\text{Im } \omega = 0$; $d = 0.5$.

Hence, for an elastic layer with a horizontal crack there exist real resonance points ω_n (more precisely, real spectral points in the space (ω, a, d)) at which the waveguide is locked up completely. Harmonic excitation at such frequencies gives rise to unlimited growth of oscillation amplitude and stress intensities at the crack edges as $t \rightarrow \infty$.

On the other hand, the resonance poles ω_n contribute in a transient motion $\mathbf{u}(\mathbf{x}, t)$ caused by a limited pulse in time $\boldsymbol{\tau}|_{z=0} = \mathbf{q}(x)f(t)$ as residues:

$$\mathbf{u}_n(\mathbf{x}, t) = \text{Re} [\mathbf{u}_n(\mathbf{x})e^{-i\omega_n t}]$$

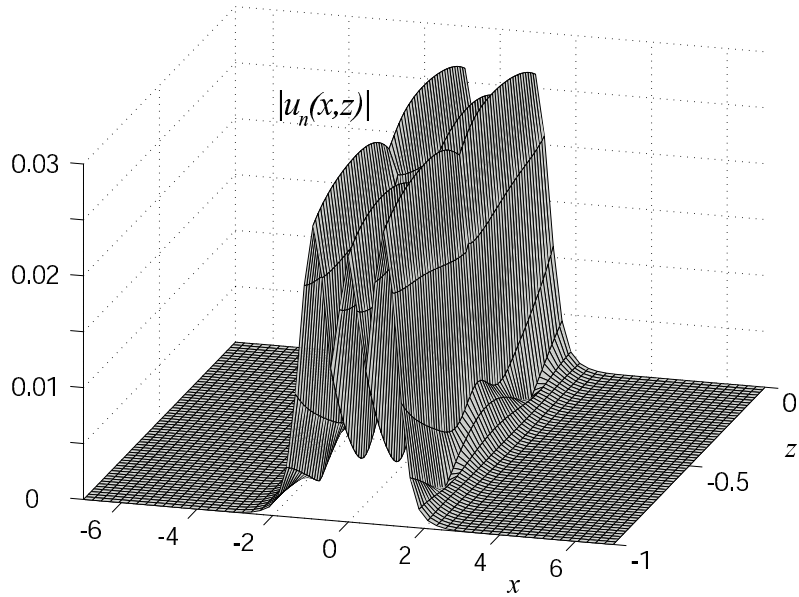


Figure 15: The amplitude of the displacement eigenform $|\mathbf{u}_n|$ at the real resonance frequency $\omega_3 = 2.17$; $a = 1.29$.

$$\mathbf{u}_n(\mathbf{x}) = -2i \operatorname{res} \mathbf{u}(\mathbf{x}, \omega)|_{\omega=\omega_n} F(\omega_n), \quad F(\omega) = \int_0^{\infty} f(t) e^{i\omega t} dt$$

The pulses related to complex ω_n decay exponentially, while a real resonance pole yields undamped harmonic oscillation, indicating the trapping of wave energy from transient signals passing by the crack.

The space distribution of the trapped oscillation is described by the complex amplitude vector $\mathbf{u}_n(\mathbf{x})$, i.e. by the displacement eigenform associated with the real spectral point ω_n . It is calculated by the same way as the reflected field \mathbf{u}_c , but via the eigenvector $\mathbf{t}_n : A(\omega_n)\mathbf{t}_n = \mathbf{0}$ instead of vector \mathbf{t} obtained from the inhomogeneous system $A\mathbf{t} = \mathbf{f}$ for the usual (non-resonant) frequencies. As is to be expected, the eigenfields $\mathbf{u}_n(\mathbf{x})$ exhibit strong space localization near the obstacle. As an example, Fig. 15 depicts the space distribution of the amplitude $|\mathbf{u}_3(x, z)|$ related to the real spectral point $\omega_3 = 2.169$, $a = 1.29$ (eigenvector \mathbf{t}_3 is normalized by the condition $|\mathbf{t}_3| = 1$). Eigenforms for all other

spectral points from the Table 3 show similar wave localization around the crack.

V. CONCLUSION

Traveling wave propagation in an elastic structure with a horizontal subsurface strip-like crack may be stopped at certain frequencies due to its diffraction by the crack. There are two kinds of blocking mechanisms:

- 1) non-resonant antiphase annihilation of the incoming wave with the diffracted one;
- 2) resonant capturing of the energy of incident waves by the eigenforms associated with the natural resonance frequencies ω_n resulting from the crack-structure wave interaction; such blocking is featured by the wave energy localization in the energy vortices formed near the crack when the oscillation frequency ω becomes close to ω_n .

The first mechanism is peculiar for the Rayleigh wave blocking in a half-plane, while it is practically impossible to meet the conditions of antiphase annihilation with two and more traveling waves excited in a free layer waveguide. It provides a full Rayleigh wave blocking ($\kappa^+ = 0$) at several (ω, d) pairs (depending on Poisson's ratio ν). The second mechanism is inherent in both half-plane and layer cases, but the examples of pure real discrete spectral points ω_n entailing the full blocking by the resonance trapping mechanism have been found only for the layer.

ACKNOWLEDGMENTS

The authors are thankful to Profs. V.A.Babeshko and D.A. Indeitsev for fruitful discussions. This work is supported by the Russian Foundation for Basic Research, project Nos. 04-01-00801 and 06-01-96607.

APPENDIX: ANALYTICAL REPRESENTATION FOR GREEN'S MATRICES K AND M

The calculation of a harmonic wave field in a layered structure by means of the Fourier transform with respect to the horizontal coordinate is brought to a multipoint boundary value problem for ordinary differential equations (ODEs) given in the sub-layers. Then the problem is reduced to a linear algebraic system arisen from the boundary conditions with respect to unknown constants of the ODE general solutions. With a few number of sub-layers this system may be solved explicitly. Hence the Fourier transform of the field in the structure can be derived analytically.

In this way the matrices K and M used in Eq. (5) are obtained via explicit representations for the sub-layers $S_1 : -d \leq z \leq 0, |x| < \infty$ and $S_2 : -H \leq z \leq -d, |x| < \infty$ into which the crack line $z = -d$ divides the initial domain $-H \leq z \leq 0, |x| < \infty$.

The integral transform $\mathbf{U}_h(\alpha, z) = \mathcal{F}[\mathbf{u}_h(x, z)]$ of a wave field \mathbf{u}_h in a layer of thickness $h: |x| < \infty, -h \leq z \leq 0$, caused by loads $\mathbf{q}^+(x)$ and $\mathbf{q}^-(x)$ applied to the surfaces $z = 0$ and $z = -h$, respectively, may be written in the following form:

$$\mathbf{U}_h(z) = K_h^+(z)\mathbf{Q}^+ + K_h^-(z)\mathbf{Q}^-, \quad -h \leq z \leq 0 \quad (\text{A1})$$

Here $\mathbf{Q}^\pm = \mathcal{F}[\mathbf{q}^\pm]$, $K_h^\pm = \|K_{h,ij}^\pm\|_{i,j=1}^2 / \Delta_h$

$$\begin{aligned} K_{h,11}^+ &= -\sigma_2[\alpha^2\gamma^2(\sigma_{12}s_2 + \gamma^2s_1) - \alpha^2\gamma^4cs_{21} + \alpha^4\sigma_{12}sc_{21} - \gamma^2\alpha^2\sigma_{12}cs_{12} + \gamma^6sc_{12}] \\ K_{h,12}^+ &= -i\alpha[-\sigma_{12}\gamma^2(\alpha^2c_1 + \gamma^2c_2) - \alpha^2\sigma_{12}^2ss_{12} + \sigma_{12}\gamma^4cc_{12} + \gamma^2\alpha^2\sigma_{12}cc_{21} - \gamma^6ss_{21}] \\ K_{h,21}^+ &= -i\alpha[\sigma_{12}\gamma^2(\alpha^2c_2 + \gamma^2c_1) - \gamma^4\sigma_{12}cc_{21} + \sigma_{12}^2\alpha^2ss_{21} - \gamma^2\alpha^2\sigma_{12}cc_{12} + \gamma^6ss_{12}] \\ K_{h,22}^+ &= \sigma_1[-\alpha^2\gamma^2(\sigma_{12}s_1 + \gamma^2s_2) + \alpha^2\gamma^4cs_{12} - \alpha^4\sigma_{12}sc_{12} + \gamma^2\alpha^2\sigma_{12}cs_{21} - \gamma^6sc_{21}] \\ \Delta_h &= 2\mu[-2\alpha^2\sigma_{12}\gamma^4 - (\gamma^8 + \alpha^4\sigma_{12})sh(\sigma_1h)sh(\sigma_2h) + 2\alpha^2\sigma_{12}\gamma^4ch(\sigma_1h)ch(\sigma_2h)] \end{aligned} \quad (\text{A2})$$

$$s_n = sh(\sigma_n z), \quad c_n = ch(\sigma_n z), \quad n = 1, 2$$

$$cs_{mn} = ch(\sigma_m h)sh(\sigma_n(h+z)), \quad m, n = 1, 2$$

$\gamma^2 = \alpha^2 - \kappa_2^2/2$, $\sigma_n = \sqrt{\alpha^2 - \kappa_n^2}$, $\kappa_n = \omega/v_n$, $n = 1, 2$, $v_1 = \sqrt{(\lambda + 2\mu)/\rho}$ and $v_2 = \sqrt{\mu/\rho}$ are P and S wave velocities in the layer material; cc_{mn} , ss_{mn} , sc_{mn} are of analogous form to sc_{mn} in which c corresponds to the hyperbolic cosine ch and s to the sine sh with the same arguments. The elements of matrix K_h^- are expressed via the elements of K_h^+ :

$$K_{h,ij}^-(z) = K_{h,ij}^+(-z-h)(-1)^{i+j-1}, \quad i, j = 1, 2$$

For brevity, we do not show the dependence on the Fourier parameter α in Eqs. (A1), (A2) above and furthermore below. We only indicate the z -dependence where it occurs.

For a half-plane ($h = \infty$) the matrix K_∞^- is unnecessary, while K_∞^+ is of much simpler form:

$$\begin{aligned} K_{\infty,11}^+ &= \sigma_2(\alpha^2 e_1 - \gamma^2 e_2), & K_{\infty,12}^+ &= i\alpha(\gamma^2 e_1 - \sigma_1 \sigma_2 e_2) \\ K_{\infty,21}^+ &= i\alpha(\sigma_1 \sigma_2 e_1 - \gamma^2 e_2), & K_{\infty,22}^+ &= \sigma_1(-\gamma^2 e_1 + \alpha^2 e_2) \\ \Delta_\infty &= 2\mu(-\gamma^4 + \alpha^2 \sigma_1 \sigma_2), & e_n(z) &= e^{-\sigma_n z}, n = 1, 2 \end{aligned} \quad (A3)$$

The matrices K and M are expressed through the matrices K_d^\pm and K_{H-d}^\pm . Indeed, for the layer under consideration

$$\mathbf{U}(z) = \begin{cases} K_d^+(z)\mathbf{Q}_0 + K_d^-(z)\mathbf{Q}, & z \in S_1 \\ K_{H-d}^+(z+d)\mathbf{Q}, & z \in S_2 \end{cases} \quad (A4)$$

Here $\mathbf{Q} = \mathcal{F}[\mathbf{q}]$ is the Fourier transform of the unknown stress vector $\mathbf{q}(x)$ at the crack plane $z = -d$. Since $\mathbf{V} = \mathbf{U}|_{z=-d-0} - \mathbf{U}|_{z=-d+0}$, Eq. (A4) yields

$$\mathbf{Q} = L\mathbf{V} + LK_d^+(-d)\mathbf{Q}_0 \quad (A5)$$

where the matrix

$$L = [K_{H-d}^+(0) - K_d^-(-d)]^{-1}.$$

Hence, in Eq. (5)

$$K(z) = \begin{cases} K_d^+(z) + K_d^-(z)LK_d^+(-d), & z \in S_1 \\ K_{H-d}^+(z+d)LK_d^+(-d), & z \in S_2 \end{cases} \quad (A6)$$

$$M(z) = \begin{cases} K_d^-(z)L, & z \in S_1 \\ K_{H-d}^+(z+d)L, & z \in S_2 \end{cases} \quad (A7)$$

For the half-plane case, obviously, K_{H-d}^+ must be replaced everywhere by K_∞^+ .

We should remark that these representations are valid with different material properties in sub-layers S_1 and S_2 (interface crack). Moreover, S_1 and S_2 may also be layered structures; in such a case K_d^\pm , K_{H-d}^\pm are calculated by certain matrix algorithms.

It is obvious that for a homogeneous layer one can take $K(z) = K_H^+(z)$ of form (A2) instead of Eq. (A6) (the latter may be reduced to (A2) in this case). Similarly, for a homogeneous half-space $K(z) = K_\infty^+(z)$ of form (A3).

References

- [1] C. M. Linton, D. V. Evans, "Trapped modes above a submerged horizontal plate," *Q. J. Mech. Appl. Math.* **44**(3), 487-506 (1991).
- [2] D. Indeitsev, "Trapping modes of oscillations in an infinitely long waveguide with submerged object in the form of a massive die," *J. Acoust. Soc. Am.* **105**(2), 1196 (1999).
- [3] I. I. Vorovich, "Resonance properties of an elastic inhomogeneous strip," *Doklady USSR* **245**(5), 1076-1079 (1979) (in Russian).
- [4] I. I. Vorovich, V. A. Babeshko, *Dynamic Mixed Problems of Elasticity for Non-classical Domains*, "Nauka, Moscow (1974) (in Russian).

- [5] C. J. S. Alves, T. Ha Duong, "Numerical resolution of the boundary integral equations for elastic scattering by a plane crack," *Int. J. Num. Mech. Eng.* **38**, 2347-2371 (1995).
- [6] A. S. Eriksson "Natural frequencies of a penny-shaped crack with spring boundary condition," *Trans. ASME. J. Appl. Mech.* **62**(1), 59-63 (1995).
- [7] Ye. V. Glushkov and N. V. Glushkova, "Resonant frequencies of the scattering of elastic waves by three-dimensional cracks," *J. Appl. Math. Mech.* **62**(5), 803-806 (1998).
- [8] Ye. V. Glushkov, N. V. Glushkova, A. V. Ekhlakov, "A mathematical model of the ultrasonic detection of three-dimensional cracks," *J. Appl. Maths Mechs*, **66**(1), 141-149 (2002).
- [9] V. A. Babeshko, E. V. Glushkov, N. V. Glushkova, and E. V. Kirillova, "Energy localization under high-frequency resonance conditions," *Sov. Phys. Dokl.* **37**(8), 443-444 (1992).
- [10] E. Glushkov and N. Glushkova, "Blocking property of energy vortices in elastic waveguides," *J. Acoust. Soc. Am.* **102**(3), 1356-1360 (1997).
- [11] E. V. Glushkov, N. V. Glushkova, and E. M. Shapar, "On the Rayleigh Wave Blocking by a Subsurface Crack," *Dokl. Phys.* **49**(10), 608-613 (2004).
- [12] E. V. Glushkov, N. V. Glushkova, and M. V. Golub, "Blocking of traveling waves and energy localization due to the elastodynamic diffraction by a crack," *Acoustical Physics*, **52**(3) (2006).

- [13] A.G. Sveshnikov "The principle of radiation," Doklady Akademii Nauk SSSR **73**(5), 917-920 (1950) (in Russian).
- [14] V. A. Babeshko, E. V. Glushkov, and N. V. Glushkova, "Energy vortices and backward fluxes in elastic waveguides," Wave Motion **16**, 183-192 (1992).
- [15] J. D. Achenbach, *Wave Propagation in Elastic Solids*, American Elsevier, Amsterdam/New York: North-Holland (1973).
- [16] P. D. Wilcox, M. J. S. Lowe, and P. Cawley, "Mode and transducer selection for long range Lamb wave inspection," J. Intelligent Mater. Syst. Struct. **12**, 553-565 (2001).
- [17] J. H. M. T. van der Hijden and F. L. Neerhoff, "Diffraction of elastic waves by a sub-surface crack (in plane motion)," J. Acoust. Soc. Am. **75**(6), 1694-1704 (1984).
- [18] G. R. Liu, "A combined finite element/strip element method for analyzing elastic wave scattering by cracks and inclusions in laminates," Comp. Mech. **28**, 76-81 (2002).